Polymer dynamics under cylindrical confinement featuring a locally repulsive surface: A quasielastic neutron scattering study

M. Krutyeva, S. Pasini, M. Monkenbusch, J. Allgaier, J. Maiz, C. Mijangos, B. Hartmann-Azanza, M. Steinhart, N. Jalarvo, and D. Richter

Citation: J. Chem. Phys. **146**, 203306 (2017); doi: 10.1063/1.4974836
View online: http://dx.doi.org/10.1063/1.4974836
View Table of Contents: http://aip.scitation.org/toc/jcp/146/20
Published by the American Institute of Physics

Polymer dynamics under cylindrical confinement featuring a locally repulsive surface: A quasielastic neutron scattering study

M. Krutyeva,[1] S. Pasini,[1] M. Monkenbusch,[1] J. Allgaier,[1] J. Maiz,[2] C. Mijangos,[2] B. Hartmann-Azanza,[3] M. Steinhart,[3] N. Jalarvo,[1,4] and D. Richter[1]
[1]*Jülich Centre for Neutron Science (JCNS) and Institute for Complex Systems (ICS), Forschungszentrum Jülich GmbH, Jülich, Germany*
[2]*Instituto de Ciencia y Tecnología de Polímeros, CSIC. Juan de la Cierva 3, Madrid 28006, Spain*
[3]*Institut für Chemie neuer Materialen, Universität Osnabrück, Barbarastraße 7, D-46069 Osnabrück, Germany*
[4]*Chemical and Engineering Materials Division, Oak Ridge National Laboratory (ORNL), P.O. Box 2008, Oak Ridge, Tennessee 37831, USA*

(Received 14 November 2016; accepted 4 January 2017; published online 2 February 2017)

We investigated the effect of intermediate cylindrical confinement with locally repulsive walls on the segmental and entanglement dynamics of a polymer melt by quasielastic neutron scattering. As a reference, the corresponding polymer melt was measured under identical conditions. The locally repulsive confinement was realized by hydrophilic anodic alumina nanopores with a diameter of 20 nm. The end-to-end distance of the hydrophobic infiltrated polyethylene-*alt*-propylene was close to this diameter. In the case of hard wall repulsion with negligible local attraction, several simulations predicted an acceleration of segmental dynamics close to the wall. Other than in attractive or neutral systems, where the segmental dynamics is slowed down, we found that the segmental dynamics in the nanopores is identical to the local mobility in the bulk. Even under very careful scrutiny, we could not find any acceleration of the surface-near segmental motion. On the larger time scale, the neutron spin-echo experiment showed that the Rouse relaxation was not altered by confinement effects. Also the entanglement dynamics was not affected. Thus at moderate confinement conditions, facilitated by locally repulsive walls, the dynamics remains as in the bulk melt, a result that is not so clear from simulations. *Published by AIP Publishing.* [http://dx.doi.org/10.1063/1.4974836]

I. INTRODUCTION

Following the rapid development of polymer systems containing all kinds of nanoparticles, the study of their physical behaviour under nanoscopic confinement has attracted significant scientific interest. Already bulk polymer melts exhibit complex dynamical properties over multiple length and time scales.[1] Thus it is highly important to understand how these complex dynamics are altered by the confinement imposed. A large variety of effects on the polymer dynamics depending on the confinement structure and the interaction between polymers and confining surface was found.[2] The investigation of polymer confinement with different geometries, polymer surface interactions, and chain sizes has become a research hotspot.

Polymer structure and dynamics are perturbed under confinement, especially when the confinement length is comparable to the size of a polymer chain (represented by the radius of gyration, R_g, or the end-to-end distance, R_e). Functional polymeric nanomaterials typically consist of nano-sized particles, which are homogenously dispersed in a polymeric matrix (nanocomposites). Extensive investigations have already been performed to explore the chain dynamics in such polymer nanocomposites.[3] For example, Li and co-workers studied the motion of unentangled polymer chains confined by non-attractive nanoparticles[4] by molecular dynamics simulations. Both normal mode and dynamic structure factor $S(Q, t)$ analysis were adopted to analyse chain dynamics. The relaxation behaviour of the chains was found to be significantly slowed down by nanoparticles. Picu and Rashit again by simulation report a uniform slowing down of the Rouse modes for neutral particles.[5] Recently Solar and Paul simulated the segmental dynamics of polybutadiene confined between graphite walls that are strongly attractive and found a strong slowing down of the corresponding alpha-relaxation close to the surface,[6,7] while in repulsive systems an acceleration of motion was found by simulation that is accompanied by a decrease of density close to the surface.[8] However other simulations arrive at accelerated motion without any change of density.[9] While for attractive surfaces, the surface influence seems to persist for several nanometers, and for repulsive surfaces, the effect is short ranged. Thus, in general, attractive up to neutral surfaces appear to slow down the relaxation, while repulsive surfaces speed it up. Finally, Anastasiadis and co-workers reviewed results on polymer dynamics under strong confinement utilizing different polymer systems where the local sub-T_g processes were found to be mostly unaffected.[10,11]

On the larger scale, confinement affects the entanglement dynamics. Studying the dynamics of polymers confined between parallel plates, Baschnagel *et al.* by simulation studied the confinement effect on the entanglement density.[12] They found that down to a plate distance corresponding to $2R_g$, no effect is visible. Li and co-workers investigated the confinement effect for walls interacting with the polymer via a Lennard–Jones potential.[13] Again disentanglement occurs around a wall distance corresponding to R_e, however, showing a broad crossover range. Very recently Kalathi *et al.* again

by a coarse-grained MD simulation analysed the polymer dynamics in nanocomposites in terms of a Rouse mode analysis.[14] They found an increase of the entanglement distance independent of the particle size, if they are in order of the tube diameter or beyond. The entanglement dilution effect was found to increase with increasing particle loading. Carrillo and co-workers presented coarse-grained molecular dynamics simulations of semi-flexible polymer melts in contact with a strongly adsorbing substrate.[15] They characterized the segments in the interfacial layer by counting the number of trains, loops, tails and non-adsorbed segments. For more rigid chains, trains originating from adsorbed segments dominate while loops are more prevalent for more flexible chains.

Some of us explored the dynamics of entangled and unentangled polymer chains in nanocomposites with the neutral or weak repulsive interaction by neutron spin echo experiments.[16–18] In particular, for entangled polyethylene-alt-propylene (PEP) polymers, they found the initial Rouse relaxation rate to be unaffected by the hydrophobic silica nanoparticles,[16] while for higher particle loading from the combined effect of geometrical and chain confinement, it was concluded that the polymers disentangle. Finally, Lin and co-workers presented experimental studies of the tracer diffusion in a polymer nanocomposite with attractive and weak interactions, suggesting that the confinement parameter alone captures the slowing down of the diffusive motion independent of segment/nanoparticle interactions.[19]

Alternatively, polymer confinement in porous media, in particular in long cylindrical nanopores, is studied frequently. As for nanocomposites, the presence of a large amount of solid surface reduces the number of possible conformations of a polymer chain and influences the dynamics, in particular for those macromolecules, which are close to the surface. Alexandris and co-workers studied the dynamics of unentangled *cis*-1,4-polyisoprene confined within self-ordered nanoporous alumina as a function of molecular weight and pore size.[20] By dielectric spectroscopy, they observed a pronounced broadening of the chain modes; the global chain relaxation was severely retarded for polyisoprenes located inside the alumina templates. Ndao and co-workers[21] reported a quasielastic neutron scattering study on nanoconfined pyrene derivative mesogenic phases. Increasing the dynamic range in combining back scattering and time-of-flight (TOF) data allowed us to evidence that within the accessible relaxation times window, the confinement of the discotic liquid crystal at the nanoscale does not modify deeply the nature of the molecular dynamics at play. From simulations, Tung and co-workers found that cylindrical nanoconfinement expands the chains conformation in the directions parallel to the confining surface while strongly compressing them normal to the surface, leading to a decrease of the entanglement density and slower local dynamics.[22] In a neutron spin-echo (NSE) study, we have shown that an attractive polymer-surface interaction leads to the formation of a surface layer, where locally the bulk dynamics persists, but on intermediate scales, the anchoring of polymer segments on the surface creates an interphase between the polymer in close vicinity to the solid surface and pure polymer.[23] In addition, at strong confinement conditions, the dilution of the entanglement network was observed.[24]

In this work, we focus on the structure and dynamics of polyethylene-alt-propylene (PEP) melts confined in cylindrical nanopores of self-ordered anodic alumina. The hydrophilic alumina surface may be considered as locally (on the length scale less than 1 nm) repulsive with respect to the strongly hydrophobic PEP. Thus, with our system, we realize the condition of a polymer under cylindrical confinement with repulsive walls. The paper is organized as follows: In Section II, we describe the theoretical background underlying our neutron scattering experiment including the basic feature of the polymer dynamics that we investigate. Thereafter we describe the experimental conditions including the production of the alumina nanopore and the polymer synthesis (Sec. III). In Sec. IV, the experimental results on the local and large scale PEP dynamics are displayed. In each case, the confined and the bulk melts are directly compared. Then in Sec. V, we discuss the results and put them into the context of simulation and other literature findings.

II. THEORETICAL BACKGROUND

A. Neutron scattering

A quasielastic neutron scattering experiment measures the double differential cross section $d^2\sigma/d\Omega d\omega$ as a function of Θ, momentum transfer $Q = \frac{4\pi}{\lambda}\sin\left(\frac{\Theta}{2}\right)$ and energy transfer $\hbar\omega$, with λ the neutron wavelength and Θ the scattering angle; for a simple one component system this reads:

$$\frac{d^2\sigma}{d\Omega d\omega} = N\left\langle\left(b-\bar{b}\right)^2\right\rangle S_{inc}(Q,\omega) + \bar{b}^2 S_{coh}(Q,\omega). \quad (1)$$

In general contributions from different constituents to the scattering functions, $S_{\mathrm{inc}}(Q,\omega)$ and $S_{\mathrm{coh}}(Q,\omega)$ must be considered, Fourier transformed, as intermediate scattering functions; this can be expressed by

$$S^{\sigma}_{inc} = \frac{1}{N_\sigma}\sum_{m}^{N_\sigma}\left\langle \exp\left[i\vec{Q}\cdot\vec{r}^{\,\sigma}_m(t)\right]\exp\left[i\vec{Q}\cdot\vec{r}^{\,\sigma}_m(0)\right]\right\rangle, \quad (2)$$

$$S^{\sigma,\delta}_{coh} = \frac{1}{\sqrt{N_\sigma N_\delta}}\sum_{m,n}^{N_\sigma,N_\delta}\left\langle \exp\left[i\vec{Q}\cdot\vec{r}^{\,\sigma}_m(t)\right]\exp\left[i\vec{Q}\cdot\vec{r}^{\,\delta}_n(0)\right]\right\rangle, \quad (3)$$

respectively, where the sums extend over all atoms (isotopes) m, n of belongings and types σ, δ in the sample. Depending on the neutron scattering lengths of the different atom types or isotopes, the scattering cross section then is

$$\frac{d\Sigma}{d\Omega}(\Theta,t) = \sum_{\sigma,\delta}\sqrt{c_\sigma c_\delta}\,b_\sigma b_\delta S^{\sigma,\delta}_{coh}(Q,t) + \sum_{\sigma} c_\sigma\left\langle\left(b_\sigma-\overline{b_\sigma}\right)^2\right\rangle S^{\sigma}_{inc}(Q,t), \quad (4)$$

with c_σ the (number) concentration of atoms of type σ in the sample.

Whereas the incoherent contribution as expressed in the second sum of Eq. (4) is universally valid, the coherent scattering—depending on Q-range, structure, and composition of the sample—may contain many cancellations of rapidly oscillating interference terms between different atoms and,

in particular in the Small Angle Neutron Scattering (SANS) regime, should be replaced by a coarse-grained version in terms of scattering length densities obtained by smearing the atomic scattering length contribution over the volume of a larger molecule segment. This leads to the common description of the SANS cross section of polymeric and other systems, where the contrast types are now labelled according to molecular groups, e.g., as in our case deuterated (D) polymer segments and protonated (H) polymer segments. With this the coherent scattering contribution reads (for a two component system)

$$\frac{d\Sigma_{coh}^{lowQ}}{\Omega}(t) \cong \frac{1}{V}\iint \Delta\varrho\left(\vec{r},t\right)\Delta\varrho(\vec{r}',0)\exp[i\vec{Q}(\vec{r}-\vec{r}')]d\vec{r}d\vec{r}', \tag{5}$$

where $\Delta\varrho\left(\vec{r},t\right)$ is the scattering length density contrast between H and D polymers for a coarse grained volume element at position r and time t. To describe polymers typically, another step of coarse graining and averaging is assumed. A polymer chain is described by a number of beads that carry the scattering length corresponding to the scattering length density contrast of the segments the beads are representing, and in a homogenous melt interferences between different chains are not correlated and cancel; the only effect of the other chains is a dilution of the effective contrast, thus

$$\frac{d\Sigma_{coh}^{lowQ}}{\Omega}(t) \cong \frac{N_{chains}}{V}\Phi(1-\Phi)\left\langle\iint \Delta\varrho(\vec{r},t)\Delta\varrho(\vec{r}',0) \times \exp[i\vec{Q}\cdot(\vec{r}-\vec{r}')]d\vec{r}d\vec{r}'\right\rangle, \tag{6}$$

where Φ is the volume fraction of one type of the chains (H or D) and $\Delta\varrho\left(\vec{r},t\right) = \sum_i^{chain}\Delta\rho\, v_{seg}\delta\left(\vec{r}-\vec{R}_{i,seg}(t)\right)$ with $\Delta\rho$ the contrast, v_{seg} the volume of a polymer segment, $\vec{R}_{seg}(t)$ the segment position, and $\delta\left(\vec{r}\right)$ the Dirac delta-function; the sum is over the segments of one chain and pointed brackets denote an ensemble average.

For typically used volume fractions, H/D contrasts, and low Q values, the intensity, i.e., the scattering contribution, of this coherent largely dominates over the incoherent contribution, which is visible as a background level in SANS.

On the other hand, the incoherent scattering that reflects the self-correlation in a protonated sample dominates the scattering over the whole Q-range due to the high incoherent cross section of protons (81 b). This applies to all backscattering (BASIS) and time-of-flight (TOF) data shown in this paper.

If we mix protonated and deuterated polymers, due to the large contrast between both species, small angle scattering from the polymer chains arises. With Neutron Spin Echo (NSE) spectroscopy, we study the large scale polymer motion as it shows itself in the pair correlation function (Eq. (6)) of a labelled chain.

Because of limited resolution of the neutron spectrometers, the measured cross sections are affected by the instrumental resolution function, which for BASIS was determined from the sample cooled to very low temperature, where all dynamical processes are frozen. Thus, the experimentally measured scattering intensity is a convolute of the true scattering function and the resolution function. In the case of NSE, which measures directly $S_{coh}(Q,t)$, the resolution correction amounts to a division by the instrumental resolution function.

B. Local dynamics as studied at BASIS

The main local relaxation (alpha-process) both in the bulk and under confinement was modelled in terms of an empirical stretched exponential or Kohlrausch–Williams–Watts (KWW) function that is known to describe the self-correlation of polymer melts very well,

$$S_{inc}^{KWW} \simeq \exp\left[-(t/\tau_{KWW})^{\beta}\right], \tag{7}$$

where τ_{KWW} is the characteristic time of the main local (segmental) relaxation of the polymer chain. In addition, PEP carries methyl groups that undergo rotational relaxation. For its description, we use the approach introduced by the Colmenero group.[25] They obtained the methyl group motion in fitting 3-fold rotational dynamics governed by a log-normal distribution of methyl relaxation rates.

Since the measurements were performed at temperatures higher than the PEP glass transition temperature ($T_g = 213$ K), the main chain motion and methyl group rotation were taken into account in the analysis,

$$S_{inc}^{H}(Q,\omega) \approx A(Q)\Big[(n_{ch} + n_{MG}EISF(Q))S_{inc}^{KWW}(Q,\omega) + n_{MG}\left(1-EISF(Q)\right)S_{QE}^{rot\&KWW}(Q,\omega)\Big] + BG, \tag{8}$$

where $S_{QE}^{rot\&KWW}(Q,\omega)$ results from a convolution of methyl group rotation and main chain relaxation, $n_{CH} = 7$ counts the H-atoms bound to the chain backbone, while $n_{MG} = 3$ relates to the methyl-group hydrogens. $A(Q) = \exp\left[-\frac{\langle u^2\rangle Q^2}{3}\right]$ is a Debye-Waller like factor that describes the missing intensity due to very fast spectral components outside the observation window. BG is a constant background describing the scattering from fast processes outside the backscattering window and instrumental background. The elastic incoherent structure factor (EISF) carries the information about the geometry of the methyl-group motion,

$$EISF = \frac{1}{3}\left(1 + 2\frac{\sin(Qr_{HH})}{Qr_{HH}}\right), \tag{9}$$

where r_{HH} is the distance between the hydrogens in the methyl group.

The log-normal distribution model characterises the hoping rates of the methyl-protons by a width σ and centre of the rate distribution Γ_0 which depends on the temperature,[25]

$$\rho(log\Gamma) = \frac{1}{\sqrt{2\pi}\sigma}\exp\left(-\frac{(log\Gamma - log\Gamma_0)^2}{2\sigma^2}\right). \tag{10}$$

Finally the observed intensity results from the convolution of the instrumental resolution function $R(Q,\omega)$ and the scattering function of the sample $S(Q,\omega)$.

In Appendix A, we illustrate how the validity of the model was corroborated by combined fits of TOF and BSS data for some of the spectra; this puts the identification of the BSS background with non-resolved fast processes on a solid ground.

C. Large scale motion as studied with NSE

At small scattering angles, NSE observes the large scale polymer dynamics in terms of the single chain dynamic structure factor that represents the single chain pair correlation function. For this more global motion, we need to distinguish two regimes: at the shorter time Rouse dynamics describe the chain motion in a heat bath, for the larger time and length scales (typically 50 Å), it is limited by the constraints and other chains are imposing on the motion on a given chain in a melt.

The Rouse model that considers a chain undergoing entropic and frictional forces in a heat bath may be solved explicitly resulting in a spectrum of characteristic times,

$$\tau_p = \frac{R_e^4}{\pi^2 W l^4 p^2}, \tag{11}$$

where R_e is the end to end distance of the chain, W the segmental relaxation rate, l the segment length, and p the corresponding eigenmodes. With both the dynamic structure factor may be calculated as

$$S_{chain}(Q,t) = \frac{1}{N}\exp\left[-Q^2 D_R t\right]\sum_{n,m}^{N}\exp\left[-\frac{1}{6}|n-m|\,Q^2 l^2\right] \times \exp\left\{-\frac{2}{3}\frac{R_e^2 Q^2}{\pi^2}\sum_{p=1}^{N}\frac{1}{p^2}\left\{\cos\left(\frac{p\pi m}{N}\right) \times \cos\left(\frac{p\pi n}{N}\right)\left(1-\exp\left(-\frac{tp^2}{\tau_R}\right)\right)\right\}\right\}, \tag{12}$$

with the Rouse time $\tau_R = \tau_{p=1}$.

Neglecting the Rouse regime, de Gennes[26] and Doi and Edwards[27] have formulated an analytic expression for the dynamic structure factor in the reptation regime that is valid for times $t > \tau_e$ once confinement effects become important ($\tau_e = {d^4}/{\pi^2 W l^4}$ is the Rouse time of a chain strand that corresponds to the entanglement distance or tube diameter d). The dynamic structure factor is composed of two contributions $S^{loc}(Q,t)$ and $S^{esc}(Q,t)$ reflecting local reptation and escape processes (creep motion) from the tube,

$$\frac{S_{chain}(Q,t)}{S_{chain}(Q,0)} = \left[1-\exp\left(-\frac{Q^2 d^2}{36}\right)\right]S^{loc}(Q,t) + \exp\left(-\frac{Q^2 d^2}{36}\right)S^{esc}(Q,t), \tag{13}$$

with $S^{loc}(Q,t)$ resulting from the longitudinal Rouse relaxation along the confining tube,

$$S^{loc}(Q,t) = \exp\left(\frac{t}{\tau_0}\right)erfc\left(\sqrt{\frac{t}{\tau_0}}\right), \quad \tau_0 = \frac{36}{W l^4 Q^4}. \tag{14}$$

For entangled chains in the NSE time window, $S^{esc}(Q, t)$ is solely influenced by contour length fluctuation (CLF) processes—creep motion out of the confining tube is not visible in the time range accessible to neutron spectroscopy.

The fluctuations of the chain ends release segments from the confining tube without creep motion of the chain center-of-mass. The first passage of a chain end relaxes the tube constraints from the end, as given in Ref. 1. The fraction of still confined segments becomes

$$\mu(t) = 1 - \frac{C}{Z}\left(\frac{t}{\tau_e}\right)^{\frac{1}{4}}, \tag{15}$$

where C ≅ 1.5 is a constant and Z the number of entanglements along the chain. Following an approach of Clark and McLeish,[28] this process may be incorporated into the structure factor of Eq. (13) resulting in

$$S^{esc}(Q,t) = \frac{N}{2\kappa^2}\Big[2\kappa + \exp(-2\kappa) + 2 - 4\kappa s(t) - 4\exp(-2\kappa s(t)) + \exp(-4\kappa s(t))\Big], \tag{16}$$

with $\kappa = {Q^2 N l^2}/{12}$ and $s(t) = 1/2(1-\mu(t))$. Since C/Z decreases with the chain length, the contribution of $S^{esc}(Q, t)$ becomes small for long chains.

III. EXPERIMENTAL

A. Sample preparation

Polyethylene-*alt*-propylene (PEP) was synthesized according to standard procedures.[29] First, isoprene was polymerized anionically using tert-butyl lithium as an initiator and cyclohexane as the solvent. The polymerization was terminated with degassed methanol. After precipitation in methanol and drying under vacuum conditions, the obtained polyisoprene was dissolved in heptane and hydrogenated using a $Pd/BaSO_4$ catalyst. The raw product was filtered, precipitated in methanol, and dried under vacuum conditions. For the protonated polymer studied at BASIS (BSS experiment), a molecular weight M_w = 28.2 kg/mol was determined by Gel Permeation Chromatography (GPC) that was equipped with a refractive index and an online light scattering detector. For the NSE experiments, another mixture of hydrogenous h- and d- PEP polymers with a molecular weight of M_w = 58.9 kg/mol for h-PEP and M_w = 64.5 kg/mol for d-PEP was synthesized in the same way. The polydispersity M_w/M_n was always not larger than 1.02.

Self-ordered nanoporous AAO, which is accessible by a two-step anodization process introduced by Masuda and Fakuda,[30] contains arrays of aligned cylindrical nanopores with narrow pore diameter distribution and uniform pore depth. The pore walls consist of hydroxyl-terminated amorphous alumina. For *NSE measurements*, self-ordered AAO with a pore diameter of 20 nm, a nearest-neighbour distance of 55 nm, and a pore depth of 100 μm (Fig. 1) was prepared following

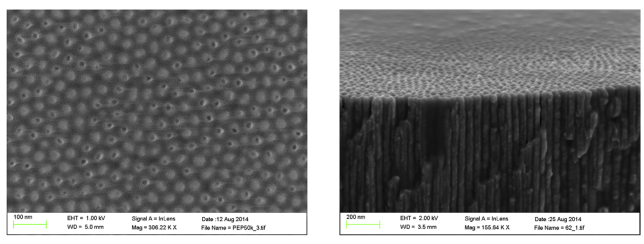

(a) (b)

FIG. 1. SEM images of surface of nanoporous Alumina infiltrated with PEP: (a) top view, (b) side view.

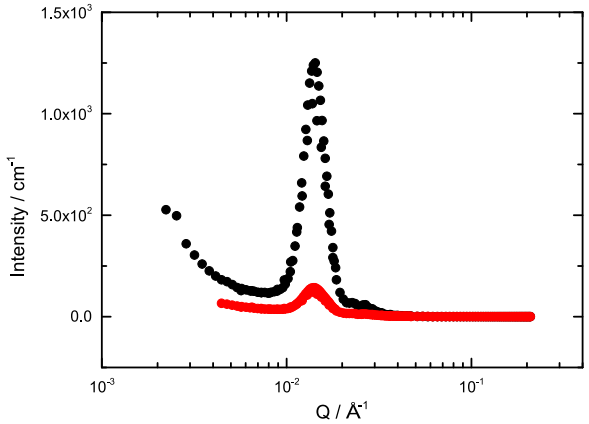

FIG. 2. Small angle scattering intensity forms the empty alumina template (black) and the template infiltrated with a matching mixture of 21.5% of protonated and 78.5% deuterated PEP. The peak intensity ratio directly reflects the degree of pore filling (88%).

a procedure reported by Jessensky *et al.*[31] The AAO layers were attached to underlying 400 μm thick Al layers so that the AAO pore bottoms were closed. The samples consisting of the AAO and Al layers were circular and had a diameter of 20 mm. 21.5% h-PEP ($M_w = 58.9$ kg/mol) and 78.5% d-PEP ($M_w = 64.5$ kg/mol) were blended, in order to match the scattering length density of AAO. This blend was named PEP50. Infiltration of the mixture was performed at 140 °C for 16 h under vacuum. Weighting of the alumina templates before and after infiltration informed about the amount of infiltrated polymer.

Small Angle Neutron Scattering (SANS) from the templates that were placed perpendicular to the incident beam was performed. For the case of infiltrated mixtures of deuterated and protonated polymer due to contrast reduction, a very clear diminution of the scattered intensity is visible, showing 88% filling of the pores. Fig. 2 compares the scattering results for both cases.

In order to investigate the integrity of the PEP melt after the scattering experiment, we measured the molecular weight distributions before and after infiltration and scattering by the GPC. Fig. 3 displays the corresponding cumulative GPC traces. The results show a small broadening of the molecular weight distribution after the NSE experiment that exerted

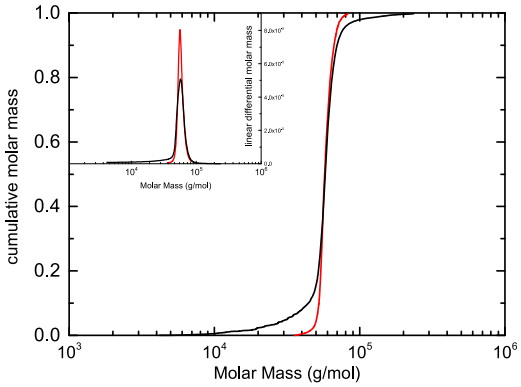

FIG. 3. Cumulative molecular mass obtained by GPC for the bulk PEP after synthesis (red) and for the PEP extracted from the pores after experiment (black). In the insert the linear differential molecular mass distributions for the same samples are shown.

the harshest conditions on the polymer. Both on the higher and the low M_w sides, some small extra contributions to the M_w distribution are visible amounting altogether to about 10% of the total. Furthermore, most of the newly created shorter chains show a molecular weight above 25 kg/mol with a very small contribution from chains between 10 and 20 kg/mol. In addition, a few percent of a molecular weight beyond about 60 kg/mol are present. Seemingly the effect of the walls maybe together with traces of oxygen let to addition—as well as to degradation—reactions that however are not detrimental neither for the experiments on segmental motion nor on the entanglement dynamics.

For *backscattering experiment*, AAO templates with a pore diameter of 20 nm and a pore length 120 μm were used. The first anodization process was carried out in 0.3M sulphuric acid, applying voltage of 20 V, for 3 h, at 0 °C. As a consequence of the first anodization, a porous alumina layer was formed. The pores of the formed alumina layer are not ordered at the free surface but are hexagonally distributed at the alumina-aluminum interface. Then, the first alumina layer was dissolved in an aqueous solution of $CrO_3 + H_3PO_4$ and the second anodization is carried out. In order to prepare an alumina template with 20 nm in pore diameter, the second anodization was carried out in 0.3M oxalic acid, applying voltage of 20 V, at 0 °C, for 168 h. The time was required to prepare nanocavities with 120 μm in length under the conditions explained.

Infiltration of PEP (M_w = 28.2 kg/mol) was performed at room temperature under vacuum conditions during a few days. Weighing of the alumina templates before and after infiltration informed about the amount of infiltrated polymer. Furthermore, confocal Raman microscopy was applied in cross sections of nanopores along the pore length demonstrating that the pores were fully infiltrated with polymer.

B. Scattering experiments

For the incoherent neutron scattering experiments, 6 membranes filled with protonated PEP were located in an aluminium container and measured at different temperatures in the interval from 170 K to 350 K at the indirect time-of-flight backscattering (BS) instrument BASIS at the SNS ORNL in Oak Ridge (USA).[32] The measurements yielded data covering an experimental energy window of ±150 μeV with an energy resolution (full width half maximum) of 3.6 μeV. The background was determined from a measurement of 2 empty templates in the aluminium container and the empty aluminium container. From the two measurements, the net scattering from the empty templates was evaluated and scaled up to the sample that contained 6 templates. Together with the empty container scattering, a reasonable background correction for the confined sample was achieved. As a reference at the same temperatures, we also studied the quasielastic scattering from a corresponding bulk melt that was background corrected by the empty container scattering. In order to achieve a reliable resolution function, we studied both samples at 40 K, where all dynamic processes that could possibly contribute to the quasielastic scattering in the instrumental window are frozen. The spectra were grouped over the detectors corresponding to scattering wave vectors Q varying from 0.2 Å^{-1} to 2 Å^{-1}. The samples were measured at two different sample orientations relative

to incident beam, 135° and 45°, allowing us to extract the dynamics perpendicular (135°) and parallel (45°) to the pore axis.

For the NSE experiments, templates of alumina with nanopores of 20 nm diameter, filled with PEP50 ((21.5% protonated and 78.5% deuterated), in order to match the scattering length density of the alumina) and then stapled inside an aluminum container have been prepared. The measurements have been performed with the NSE spectrometers at SNS ORNL in Oak Ridge (USA), at MLZ in Garching (Germany) and at ILL in Grenoble (France). In addition to the confined polymer, a sample (bulk) of the same PEP 50 kg/mol in Nb container has been measured at SNS and ILL. The NSE measurements have been performed at a temperature of 420 K, for Fourier times up to 250 ns and at different values of the momentum transfer Q. In order to minimize the background due to the Bragg-peak scattering from the pores, all samples (i.e., confined and bulk polymers as well as resolution and background samples) have been measured with the sample rotated by 30°. Thus the reciprocal space plane containing the scattering contribution of the elongated straight pores no longer coincides with the tangential plane of the Ewald sphere containing the experimental Q vectors.

IV. EXPERIMENTAL RESULTS

A. Segmental motion

Following Sec. II, we analysed the spectra obtained from BASIS in terms of a Kohlrausch-William-Watts function combined with the methyl group scattering. The methyl group parameters (temperature dependent relaxation rate Γ_0 and distribution width σ) were taken from the work of Aparicio *et al.*[25] Furthermore, we assume the absence of any confinement effect on the methyl group rotation. Here we follow the literature results such as those on the confined dynamics of poly(methyl phenyl siloxane) in layered nano-hybrides by quasielastic neutron scattering, where the methyl group rotation was found to be unaffected even by the severe confinement,[33] or the various results on methyl group rotation in asymmetric polymer blends, where the slow component acts as a confining matrix.[34,35]

The stretching exponent was fixed to be $\beta = 0.53$, a common value for polymer melts in the segmental relaxation regime and in agreement with Ref. 25. The evaluation focused on the Q-range $1.0 \le Q \le 1.4$ Å^{-1}. In this Q-range in polymer melts and in particular in PEP,[25] the quasielastic width scales with $\tau_{KWW} \sim Q^{-2}$. Keeping this in mind and in order to achieve stable fits that allowed us to signify small differences in τ_{KWW}, combined fits were performed that kept the Q-dependence of the relaxation time fixed to Q^{-2}. Also the methyl group contribution was not varied. Furthermore, for each spectrum, a constant background was allowed for that accounted for fast vibrational and librational processes in the material (see Appendixes A and B). As an example Fig. 4 presents the corrected quasielastic spectra from the bulk sample (a) and the confined material (b) for 3 Q-values at 300 K at 135° sample orientation. Since the segmental displacements perpendicular to the pore axis are more sensitive to the confinement, the measurements at 135° sample orientation were preferably

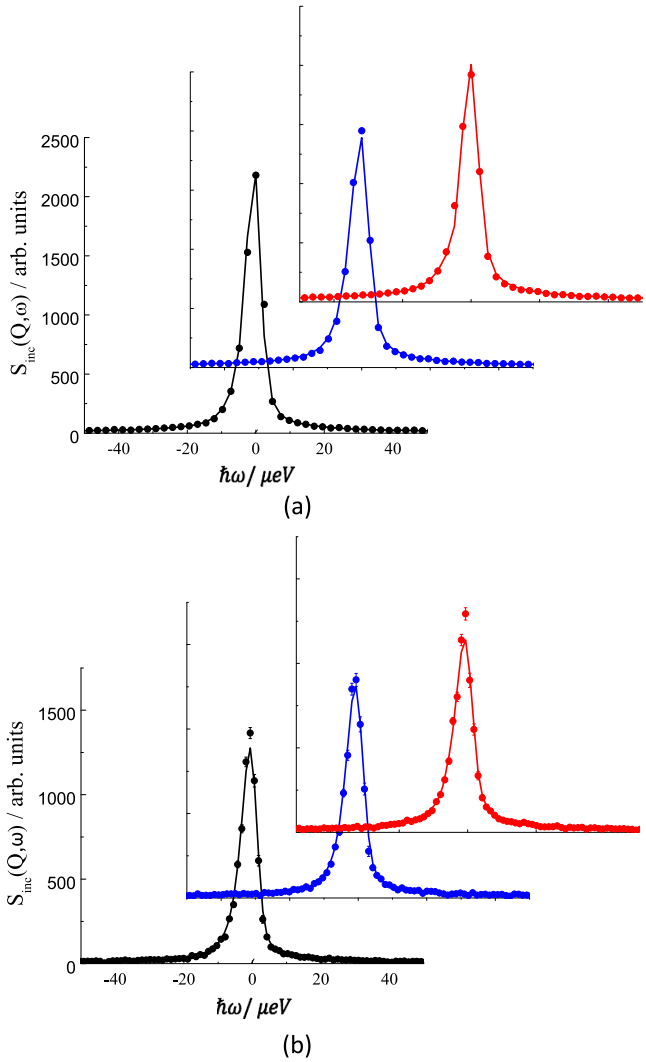

FIG. 4. Background subtracted BS spectra for bulk PEP (a) and confined PEP (b) at 300 K obtained for Q = 1.0 Å^{-1} (black), Q = 1.2 Å^{-1} (blue), and Q = 1.4 Å^{-1} (red). Lines are the fitting curves with the model Eq. (8).

analysed. The data for 45° sample orientation are not presented here. Fig. 4 includes the fit results and demonstrates the very high quality of the fits. Fig. 5 displays the temperature dependent spectra for a selected Q value (Q = 1.4 Å^{-1}). Again the good quality of the fits is evident. Finally Table I presents the results for the characteristic time τ_{KWW} measured for bulk and confined PEP.

The fitting results of main chain relaxation time τ_{KWW} obtained by BS are comparable with the literature data.[25] In order to place our results into the context of earlier results, we also performed separate spectral fits over the full Q-range. The results for τ_{KWW} at 325 K are shown in Fig. 6 and are compared with the bulk literature data of Aparicio *et al.*[25] As may be seen both data sets agree very well. Fig. 7 compares the spectra from the confined polymer measured at Q = 0.8 Å^{-1} with that obtained at Q = 1.4 Å^{-1} measured at 250 K. Even there the dispersion with Q is clearly visible.

As Table I shows that the difference between the bulk relaxation and that for the confined material is very small, with if at all a slight tendency to slower relaxation under confinement and low temperatures.

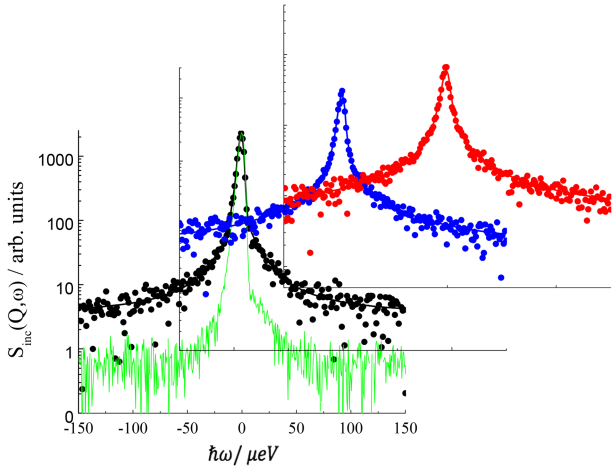

FIG. 5. Background subtracted BS spectra of confined PEP measured at different temperatures: 250 K (black), 300 K (blue), 325 K (red), and 40 K (green) illustrating the shape of the resolution. The data for Q = 1.4 Å^{-1} are presented. The lines represent the results of the fitting with Eq. (8).

TABLE I. Temperature dependent results for τ_{KWW} (Q = 1.0 Å^{-1}) as obtained from the combined fits: τ_{KWW}^{bulk} for the bulk PEP; τ_{KWW}^{conf} for the confined PEP. The overall systematic errors of the derived τ_{KWW} values considering uncertainties in the background from very fast processes and the exact nature and form of the fast process are estimated to be about 10% (see Appendix A).

Temperature (K)	τ_{KWW}^{bulk} (ns)	τ_{KWW}^{conf} (ns)
250	31.3 ± 0.1	32.3 ± 1.1
280	4.76 ± 0.05	5.2 ± 0.4
300	1.17 ± 0.01	1.37 ± 0.06
325	0.35 ± 0.01	0.36 ± 0.05
350	0.098 ± 0.002	0.10 ± 0.02

B. Entanglement dynamics

Fig. 8 displays the NSE results for bulk PEP at 420 K. In order to determine the Rouse rate Wl^4 (see Eqs. (8) and (9), we analysed the data of the bulk sample in the early time regime, where entanglement does not yet affect the dynamic structure factor. We fitted the experimental data for times shorter than 10 ns with the Rouse model (Eq. (9)) varying only the Rouse rate Wl^4. The solid lines in Fig. 8 display the

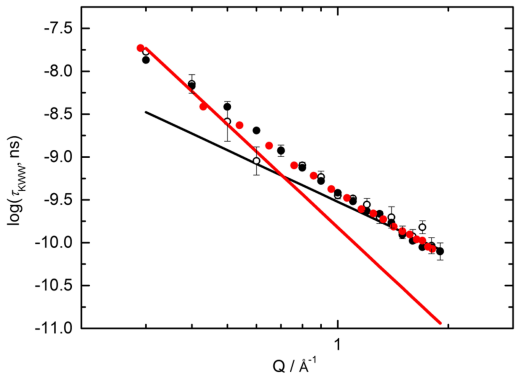

FIG. 6. Dependence of the main chain relaxation time on the momentum transfer for the confined PEP (open black symbols), bulk PEP (filled black symbols), and data from the literature[25] (red symbols) at the temperature 325 K. Red line is power law Q^{-4}; black line is power law Q^{-2}. For the bulk and confined PEP, the statistical error is presented.

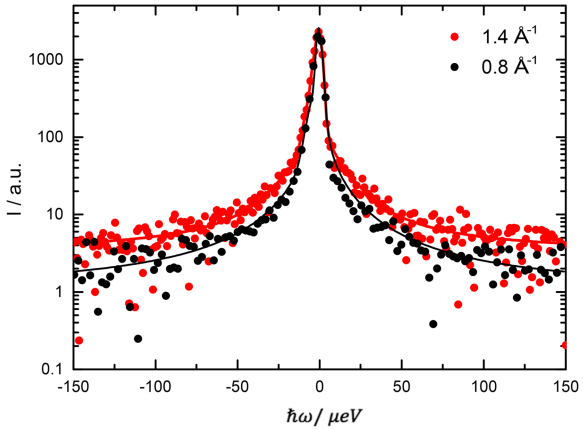

FIG. 7. Background subtracted BS spectra of confined PEP at 250 K for different Qs. Fitting with the stretched exponential function is presented by solid lines.

outcome. We obtain Wl^4 = (1.10 ± 0.02) nm^4/ns that compares well with Wl^4 = 0.95 nm^4/ns for PEP at 423K known from the literature.[36]

Before we can start analyzing the effects of confinement on the entanglement dynamics, the contribution coming from the background must be taken into account and subtracted. First, the empty cell was measured with the NSE spectrometer and its contribution subtracted from the $S(Q, t)$ during the data reduction. However, the cell alone is not the only (and main) source of background in our system. As has been thoroughly investigated in Ref. 24 in general, the pores are very difficult to fill completely with polymer. Thus even under contrast matching condition, there is a severe pore scattering. This extra scattering may be significantly reduced in turning the sample plane away from a perpendicular direction towards the beam. Then the Ewald sphere of experimental Q-values (exactly its tangential plane) no longer coincides with the reciprocal space plane of the scattering from the hexagonal array of pores, but is turned away from it in scattering plane. Still some residual scattering remained that may be related to some disorder in the pore lattice and incomplete filling. Therefore, in addition to the tilting, we took a specific route to eliminate the residual background contribution: In the light of the results from the measurements on the local dynamics by backscattering, we know that the Rouse rate hardly changes under confinement; with that we can estimate how much background needs to be

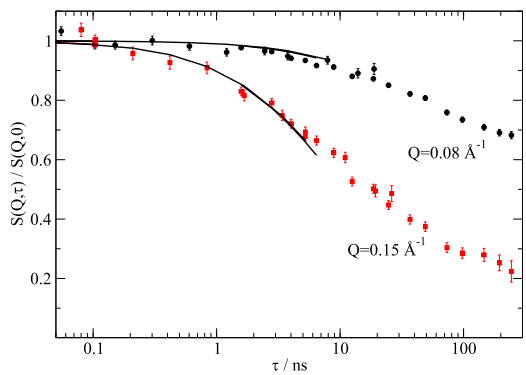

FIG. 8. NSE experimental data for PEP bulk polymer fitted with the Rouse model.

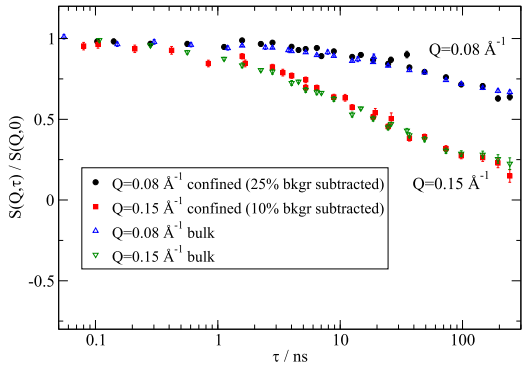

FIG. 9. PEP bulk and PEP confined data plotted together, the latter after subtraction of the background (see text). For sake of clarity only the experimental data from SNS-NSE and ILL-IN15 are shown.

subtracted from the PEP-data under confinement in order to find the same dynamics at short Fourier times as for the bulk. We adopted the following procedure: We first subtracted the background from the NSE data and then rescaled the curve to one 1 for $t \to 0$. The best match at short Fourier times between the two curves (i.e., confined vs. bulk data) was obtained for a background of 25% for Q = 0.08 Å^{-1} and 10% for Q = 0.15 Å^{-1}.

After background subtraction from the pores and the rescaling, Fig. 9 shows how the data for confined and bulk lie on top of each other, not only in the Rouse regime, but also for $t > \tau_e \sim 50$ ns, in the local reptation regime. Thus, we do not see any evident effects of the confinement on the polymer dynamics. In this regime, we fitted the tube diameter d by using Eq. (15) with C = 1.5 that includes contour length fluctuation contributions. For PEP in bulk, we find $d = 47.3 \pm 0.4$ Å. From the fitting of the tube constraints for PEP under confinement imposing the same Rouse rate as for the bulk and we find $d = 48.7 \pm 0.5$ Å, see Fig. 10. Within experimental error, both results for the tube constraints are virtually the same. Recently by a direct measurement of the CLF effect using ring polymers as a probe, we found that the contribution of CLF was weaker than theoretically predicted (C = 1.1 instead of C = 1.5).[37] Then less segments are freed by CLF, and consequently for a given experimental result the tube constraints need to come out somewhat more relaxed. Using C = 1.1, we refitted the data resulting in $d = (52.5 \pm 0.5)$ Å for the bulk and $d = (52.8 \pm 0.6)$ Å for the confined polymer.

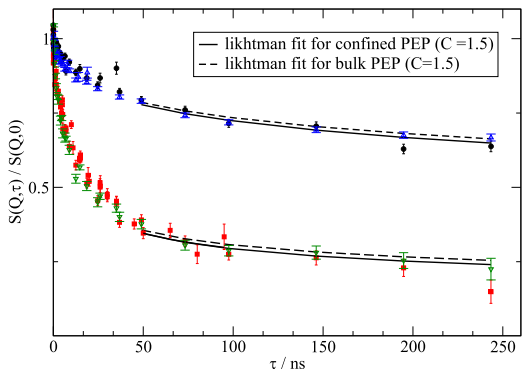

FIG. 10. Experimental data from SNS-NSE, ILL-IN15, and J-NSE for PEP bulk and PEP in confinement as in Fig. 9 but fitted with the Likhtman model (C = 1.5) for $t > \tau_e$.

Within experimental error our experiments find that the reptation tube diameter is not affected by the confinement in nanopores featuring a pore diameter comparable to the end to end distance of the confined chain.

V. DISCUSSION

In this work, we have investigated the local (segmental) dynamics as well as the entanglement dynamics of PEP, a strongly hydrophobic polymer confined in alumina nanopores featuring polar surfaces that lead to hard wall repulsion with negligible local attraction. The size of the confining pores was very close to the end-to-end distance of the polymer. At $M_w = 58.9$ kg/mol and 28.2 kg/mol with $R_e^2 = C_\infty n l^2 N$, $C_\infty = 7$,[38] n = 3.84, and N = 866 and 415, we have $\sqrt{R_e^2} = 23.5$ nm (NSE sample) and 16.6 nm (BSS sample), i.e., of order of the pore diameter of 20 nm. Thus, we have dealt with a polymer under moderate confinement conditions with locally repulsive walls.

A. Main chain relaxation

In the investigated temperature interval, above the glass transition temperature, on a local scale, the main dynamical process is the structural relaxation of monomer units (α-relaxation). In Fig. 6 we have shown the overall Q-dispersion of the characteristic Kohlrausch-Williams-Watts (KWW) relaxation time τ_{KWW} and compared it with Aparicio's results. We realize that our new results taken in a larger dynamic window (±150 μeV compared to ±16 μeV) agree very well with the older data. We also observe the crossover from the Rouse dynamics at low Q, where the Gaussian behaviour with $\tau_{KWW} \propto Q^{-2/\beta} \propto Q^{-4}$ prevails, to a weaker Q-dependence $\tau_{KWW} \propto Q^{-2}$ at Q-values above about Q = 1.0 Å^{-1} (Fig. 6). Also the observed temperature dependence agrees well with earlier results (Fig. 11). The apparent activation energy derived from the temperature dependence of τ_{KWW} amounts to about 41 KJ/mol again close to the literature value for bulk PEP.[25]

The simulation for systems confined with repulsive walls[6,8,9] predicts accelerated relaxation; however, in our case the spectra from the confined polymer gave rise to nearly identical relaxation times as those of the pure bulk melt. As

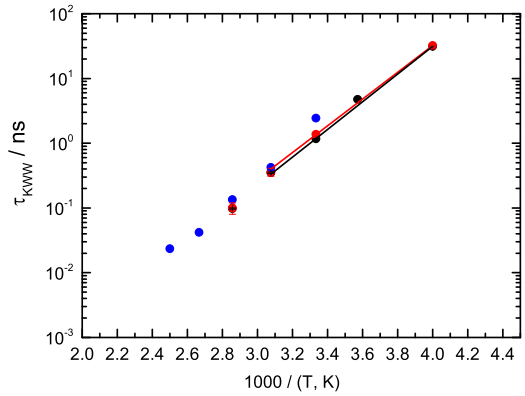

FIG. 11. Dependence of the relaxation times on the temperature (Table I) for the bulk PEP (black symbols), confined PEP (red symbols) together with the literature data (blue).[25] Solid lines represent fitting with exponential function resulted in the activation energy (see text).

Table I shows, at a lower temperature, the confined relaxation times came out slightly longer, however, at the limit of statistical accuracy. For a quest towards the near surface relaxation behaviour, in a second step we assumed that inside the pore the relaxation is bulk like with the parameters obtained for the reference sample and that only the outermost 1 nm polymer layer is affected by the surface. Here we follow the simulation result that for locally repulsive walls, the surface effect diminishes quickly towards the samples interior.[39] For our pore size of 20 nm, this would affect a polymer volume fraction of 20%. However, fitting the data with two components, where with 80% volume fraction the dynamics was assumed bulk like and for 20% the relaxation time was allowed to vary freely, within statistical accuracy, the relaxation behaviour of this surface layer could not be distinguished from the bulk.

In simulations a faster motion of the polymer segments or beads close to a repulsive surface were observed at several instances. For example, Varnik *et al.*[9] found significantly larger mean square displacements for segments in the first two adjacent layers close to the wall compared to those in the interior of the material. Smith *et al.*[8] related the increase of the segmental mobility in the neighbourhood to a repulsive wall to a reduced segment density. In free standing films such a density reduction is even more pronounced with an even larger effect on the mobility increase close to the surface.[40] Our experiments do not support such an effect, even though the strongly hydrophilic alumina should be a good experimental realization of a strongly locally repulsive wall for a hydrophobic hydrocarbon.

B. Entanglement dynamics

With the same objective, we also explored the Rouse and entanglement dynamics of PEP in nanoconfinement by NSE spectroscopy and compared the results with melt data that were obtained under identical conditions. Since the experiments needed to be performed in the low Q-regime, great care was taken to master the influence of the template scattering. From the study of the main chain relaxation, we knew that there was a very little difference between the segmental relaxation in bulk and under confinement. The evaluation of the data in the up to 10 ns regime, the Rouse regime, confirmed the BASIS data interpretation, as under both conditions, bulk melt and confined polymer within the experimental error display an identical relaxation behaviour (Fig. 10). Thus by and large the monomeric friction did not change. The result of unchanged Rouse modes differs significantly from what is found for neutral surfaces, where simulations observed a slowing of all Rouse modes.[5,13]

Already Fig. 9 demonstrates that the long-time relaxations under bulk and confinement conditions are identical within experimental accuracy. Quantitatively the tube diameter was determined in terms of the structure factor including CLF (Eq. (15)). The result of $d \cong 48$ Å needs to be compared with earlier studies that revealed $d = 60$ Å at 492 K[41] implying a significant T-dependence of the constraints. We note that in a very early study on temperature dependent constraints in PEP melts, about 20% change of tube diameter between 423 K and 492 K was reported[42] in quite good agreement with the present result.

Our experiment shows that intermediate confinement between locally repulsive walls does not affect the entanglement network. This finding agrees with the early results of Baschnagel *et al.*,[12] who reported from simulations of chains between two flat repulsive walls that for a wall distance of $2R_g$ the entanglement distance hardly changes. On the other hand, Li *et al.*[13] reported again the disentanglement phenomenon for plate distances corresponding to R_e, however, displaying a broad crossover regime. Our results imply an unaffected entanglement distance for $R_e \cong$ nano-tube diameter ϕ, implying that the onset of a broad cross over regime would have to be shifted to a stronger confinement. We remark that for strong confinement conditions accompanied by attractive walls (poly(ethylene oxide) in nanopores) NSE experiments showed that at $R_e = 2.5\,\phi$ the tube diameter increases by merely 10%.[24]

C. Summary and conclusions

We have studied the dynamics of PEP confined rigid nanopores of self-ordered nanoporous alumina, providing hard wall repulsion with negligible local attraction, in a broad temperature interval by quasielastic neutron scattering employing backscattering and NSE. As a reference we investigated a bulk PEP melt under identical conditions. The following results stand out: (i) in the regime of segmental dynamics even though expected on the basis of simulations, we observe virtually no effect of the confining walls on the local segment relaxation. (ii) Concerning the larger scale Rouse and entanglement dynamics within experimental accuracy, both the Rouse relaxation rate and the entanglement distance do not differ between bulk and confined polymer melts. The experiments clearly show that for a confinement size equalling the polymer end-to-end distance R_e, the entanglement network is not affected, a result that is not so clear from simulations.

ACKNOWLEDGMENTS

The authors thank instrument responsible Michael Ohl (SNS@ORNL), Oxana Ivanova (MLZ@FRM-II), Olaf Holderer (MLZ@FRM-II), Aurel Radulescu (MLZ@FRM-II), Tobias Unruh (MLZ@FRM-II[46]), and Peter Falus (ILL) for help with neutron scattering experiments. The financial support of DFG Priority Program SPP1369 (Project Nos. KR 3929/1-1 and STE 1127-9) and Grant Nos. FPI BES-2009-026632 and MAT2014-53437-C2-1P is gratefully acknowledged. The research at ORNL's Spallation Neutron Source was sponsored by the Scientific User Facilities Division, Office of Basic Energy Sciences, U.S. Department of Energy.

APPENDIX A: COMBINED TOF AND BASIS DATA ANALYSIS

The reliability of parameter extraction from backscattering spectra depends on the proper treatment of fast components that mainly contribute to an observed intensity offset (background). Depending on the assumption of the background level, the values obtained for the characteristic time of the slow component τ_{KWW} may vary. Thus a reliable method to

independently fix this background is essential to corroborate the evaluation procedure of the backscattering spectra. The background may consist in a small amount of residual environmental background scattering or other unspecified sources. However, the dominant part stems from fast processes with spectral widths that extend significantly beyond the backscattering observation window (for BASIS: −150/ns $< \omega <$ −150/ns or −100 μeV $< \hbar\omega <$ 100 μeV). One part of the fast contribution pertains to the well-established rotational jump diffusion of CH_3 groups (see Eqs. (9) and (10)) and further contributions stem from fast local segment motions, e.g., the β-relaxations. The inclusion of TOF data covering the range −2000/ns $< \omega <$ −2000/ns (−1.3 meV $< \hbar\omega <$ 1.3 meV) allows for an explicit spectrum modelling of these components. Figure 12 illustrates how the intensity values at the boundary of the spectrum relate to the quasielastic components seen with TOF. Beyond that very broad spectral components from molecular vibrations, librations and phonon-like excitations will be present that still contribute a small(er) virtually constant background even on the here available TOF range.

The methodology for combined fitting of data from different instruments using proper resolution models in each case has been described in Refs. 43 and 44. The individual resolution functions have been modelled by up to 8 Gaussians (necessary for BASIS data) to the scattering from the cold (T < 40 K) samples. The Gaussians are used in the integration kernels for the Fourier transforms which convert the KWW and related function (Eq. (7)) to the time domain. The thus computed spectrum (Eq. (8)) then automatically contains the proper resolution broadening. The data, which are combined, were obtained with BASIS for −150/ns < ω < −150/ns and from TOF in the range from −2000/ns < ω < −2000/ns and for 3 Q-values 1.0, 1.2, and 1.4 Å^{-1}. In order to keep the number of parameters low, we assumed $\tau_{KWW} = \tau_{KWW}\left(Q = 1.0\,\text{Å}^{-1}\right) Q^{-2}$ and a common τ_{fast} associated with a stretched exponential time function with $\beta = 0.5$. The fast component was assumed without Q-dispersion but with an EISF approximated as $EISF2 = \exp\left(-\frac{1}{3}\left(r_f Q\right)^2\right)$, thus replacing the BG in Eq. (8) by a convolution with $\left[EISF2 + (1 - EISF2)\, S_{fast}(Q,\omega)\right]$, which technically is realised by multiplication with $[EISF2 + (1 - EISF2)]\exp(-\left\{\tau_{fast}\right\}^{\beta}]$ and subsequent Fourier transform in the time domain. By computing the integral over each frequency channel width also, steep and narrow spectral features are always treated properly. All residual effects are represented by small background contributions, which were assumed the same for all Q's but different for TOF and BS.

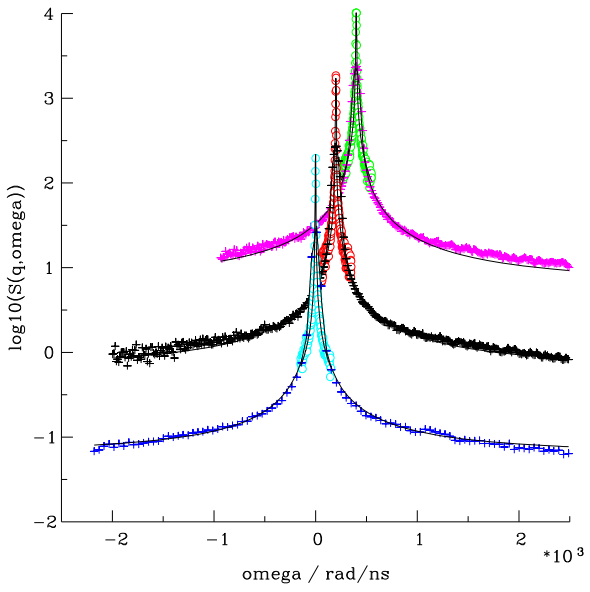

FIG. 12. Time-of-flight (+) and backscattering (∘) spectra of the bulk polymer with the combined fit for both spectrometers and Q = 1.0, 1.2, and 1.4 Å^{-1} measured at T = 300 K, curves for subsequent Q's are shifted by 200/ns and multiplied by factor 10 for better discrimination. Residual constant background levels are 0.06 and 0.1, respectively, on the displayed scale.

The combined fit for bulk PEP at T = 300 K consistently with Ref. 25 and our BASIS based evaluation yields τ_{KWW} = 1.03 ns, $\ln(\tau_{MG}) = -3.85$, $\tau_{fast} = 0.0018$ ns, and $r_f = 0.73$ Å, u^2 =0.344 Å^2. In addition, the TOF data are scaled by 0.82 for best fitting. (This may be attributed to temperature and wavelength dependence of the self shielding of the sample.) Analogous treatment of the T = 350 K data yields $\tau_{KWW} = 0.11$ ns again in accordance with Table I.

Whereas the parameters of the fast component and the methyl group rotation are somehow correlated and less well defined, the extracted τ_{KWW} values are robust and significant.

APPENDIX B: SANS

Information on the structure of the polymer inside the pores can be extracted from the SANS measurements. However, this information is limited in accuracy due to the uncertainties in background subtraction. The inset in Fig. 13 shows the SANS measurements on PEP in AAO under three different orientations of the sample: Sample perpendicular to the beam and pores aligned along the beam (black) and sample (and pores) rotated to about −30° and +30° (red and green) with respect to the perpendicular position. If one observes the curves in the inset for the rotated sample one can notice that (a) some residual scattering from the pore is still present (small peak at Q ~ 0.015 Å^{-1}) and (b) a background effect can be seen at very large Q's.

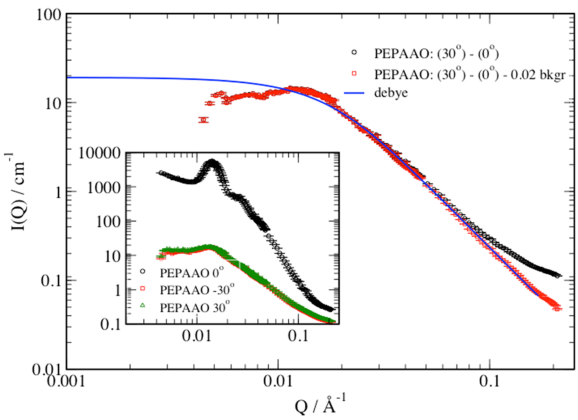

FIG. 13. SANS data for the alumina template infiltrated with d/h PEP mixture measured at 30° after background subtraction (see text). Inset: SANS data obtained at 0° (black), 30° (green), and −30° (red) sample rotation relative to the perpendicular position.

Starting from these observations, we subtracted from one of the datasets for the rotated sample (i.e., PEPAAO 30°) the contribution of the perpendicular sample, the latter rescaled to the intensity of the former; the result is the black curve of the main figure (PEPAAO 30°–0°). From this curve we roughly estimate the residual background and subtracted a corresponding constant level from the data and obtained the red curve of the main figure (PEPAAO 30°–0°-2%). This can be fitted with the Debye model (with modified chain statistics[45]) with the radius of gyration (R_g) as a free parameter. We find $R_g = 85$ Å. For PEP bulk, we expect an end-to-end radius of circa $R_e = 235$ Å yielding an unperturbed $R_g = R_e/\sqrt{6} \sim 96$ Å.

Given the amount of polymer in the beam determined from the weight changes of the platelets upon infiltration, we determined the expected absolute scattering intensity scale for the polymer scattering and fixed it during fitting. The chain statistics—as indicated by the exponent of the asymptotic Q-dependence ($1/Q^{\nu}$)—deviates from the Gaussian value and is rather $\nu = 2.3$ instead of 2. Thus the shape of polymer scattering indicates some degree of compression. The scattering geometry in the SANS experiment was such that the direction perpendicular to the confining pore surfaces was probed. Whereas the deviation of the exponent seems robust against details of the background subtraction, the value of R_g is less well defined due to the residues of pore scattering intensity in the low Q region.

[1] T. C. B. McLeish, Adv. Phys. **51**, 1379 (2002).
[2] G. B. McKenna, Eur. Phys. J.: Spec. Top. **189**, 285 (2010).
[3] A.-C. Genix and J. Oberdisse, Curr. Opin. Colloid Interface Sci. **20**, 293 (2015).
[4] Y. Li, M. Kröger, and W. K. Liu, Soft Matter **10**, 1723 (2014).
[5] R. C. Picu and A. Rakshit, J. Chem. Phys. **126**, 144909 (2007).
[6] M. Solar, L. Yelash, P. Virnau, K. Binder, and W. Paul, Soft Mater. **12**, S80 (2014).
[7] M. Solar, E. U. Mapesa, F. Kremer, K. Binder, and W. Paul, Europhys. Lett. **104**, 66004 (2013).
[8] G. D. Smith, D. Bedrov, L. Li, and O. Byutner, J. Chem. Phys. **117**, 9478 (2002).
[9] F. Varnik, J. Baschnagel, and K. Binder, Phys. Rev. E **65**, 21507 (2002).
[10] K. Chrissopoulou and S. H. Anastasiadis, Soft Matter **11**, 3746 (2015).
[11] K. Androulaki, K. Chrissopoulou, D. Prevosto, M. Labardi, and S. H. Anastasiadis, ACS Appl. Mater. Interfaces **7**, 12387 (2015).
[12] H. Meyer, T. Kreer, A. Cavallo, J. P. Wittmer, and J. Baschnagel, Eur. Phys. J.: Spec. Top. **141**, 167 (2007).
[13] Y. Li, D. Wei, C. C. Han, and Q. Liao, J. Chem. Phys. **126**, 204907 (2007).
[14] J. T. Kalathi, S. K. Kumar, M. Rubinstein, and G. S. Grest, Soft Matter **11**, 4123 (2015).
[15] J.-M. Y. Carrillo, S. Cheng, R. Kumar, M. Goswami, A. P. Sokolov, and B. G. Sumpter, Macromolecules **48**, 4207 (2015).
[16] G. J. Schneider, K. Nusser, L. Willner, P. Falus, and D. Richter, Macromolecules **44**, 5857 (2011).
[17] K. Nusser, G. J. Schneider, and D. Richter, Soft Matter **7**, 7988 (2011).
[18] T. Glomann, G. J. Schneider, J. Allgaier, A. Radulescu, W. Lohstroh, B. Farago, and D. Richter, Phys. Rev. Lett. **110**, 178001 (2013).
[19] C.-C. Lin, S. Gam, J. S. Meth, N. Clarke, K. I. Winey, and R. J. Composto, Macromolecules **46**, 4502 (2013).
[20] S. Alexandris, G. Sakellariou, M. Steinhart, and G. Floudas, Macromolecules **47**, 3895 (2014).
[21] M. Ndao, R. Lefort, C. V. Cerclier, R. Busselez, D. Morineau, B. Frick, J. Ollivier, A. V. Kityk, and P. Huber, RSC Adv. **4**, 59358 (2014).
[22] W.-S. Tung, R. J. Composto, R. A. Riggleman, and K. I. Winey, Macromolecules **48**, 2324 (2015).
[23] M. Krutyeva, A. Wischnewski, M. Monkenbusch, L. Willner, J. Maiz, C. Mijangos, A. Arbe, J. Colmenero, A. Radulescu, O. Holderer, M. Ohl, and D. Richter, Phys. Rev. Lett. **110**, 108303 (2013).
[24] J. Martín, M. Krutyeva, M. Monkenbusch, A. Arbe, J. Allgaier, A. Radulescu, P. Falus, J. Maiz, C. Mijangos, J. Colmenero, and D. Richter, Phys. Rev. Lett. **104**, 197801 (2010).
[25] R. P. Aparicio, A. Arbe, J. Colmenero, B. Frick, L. Willner, and D. Richter, Macromolecules **39**, 1060 (2006).
[26] P. G. De Gennes, J. Phys. **42**, 735 (1981).
[27] M. Doi and S. F. Edwards, *The Theory of Polymer Dynamics* (Clarendon Press Oxford, Oxford, 1986).
[28] N. Clarke and T. C. B. Mcleish, Macromolecules **26**, 5264 (1993).
[29] J. Allgaier, A. Poppe, L. Willner, and D. Richter, Macromolecules **30**, 1582 (1997).
[30] H. Masuda and K. Fukuda, Science **268**, 1466 (1995).
[31] O. Jessensky, F. Müller, and U. Gösele, Appl. Phys. Lett. **72**, 1173 (1998).
[32] E. Mamontov and K. W. Herwig, Rev. Sci. Instrum. **82**, 085109 (2011).
[33] K. Chrissopoulou, S. H. Anastasiadis, E. P. Giannelis, and B. Frick, J. Chem. Phys. **127**, 144910 (2007).
[34] M. Tyagi, A. Arbe, A. Alegría, J. Colmenero, and B. Frick, Macromolecules **40**, 4568 (2007).
[35] A. Arbe, A. Alegría, J. Colmenero, S. Hoffmann, L. Willner, and D. Richter, Macromolecules **32**, 7572 (1999).
[36] D. Richter, M. Monkenbusch, A. Arbe, and J. Colmenero, *Neutron Spin Echo in Polymer Systems* (Springer Berlin Heidelberg, Berlin, Heidelberg, 2005).
[37] S. Gooßen, M. Krutyeva, M. Sharp, A. Feoktystov, J. Allgaier, W. Pyckhout-Hintzen, A. Wischnewski, and D. Richter, Phys. Rev. Lett. **115**, 148302 (2015).
[38] A. Zirkel, D. Richter, W. Pyckhout-Hintzen, and L. J. Fetters, Macromolecules **25**, 954 (1992).
[39] S. Peter, S. Napolitano, H. Meyer, M. Wübbenhorst, and J. Baschnagel, Macromolecules **41**, 7729 (2008).
[40] A. R. C. Baljon, S. Williams, N. K. Balabaev, F. Paans, D. Hudzinskyy, and A. V. Lyulin, J. Polym. Sci., Part B: Polym. Phys. **48**, 1160 (2010).
[41] A. Wischnewski, M. Monkenbusch, L. Willner, D. Richter, and G. Kali, Phys. Rev. Lett. **90**, 58302 (2003).
[42] D. Richter, B. Farago, R. Butera, L. J. Fetters, J. S. Huang, and B. Ewen, Macromolecules **26**, 795 (1993).
[43] A. Stadler, M. Monkenbusch, R. Biehl, D. Richter, and J. Ollivier, J. Phys. Soc. Jpn. **82**, SA016 (2013).
[44] M. Monkenbusch, A. Stadler, R. Biehl, J. Ollivier, M. Zamponi, and D. Richter, J. Chem. Phys. **143**, 75101 (2015).
[45] H. C. Benoit, Compt. Rend. **245**, 2244 (1957).

[46] Present address: Friedrich-Alexander-Universität Erlangen-Nürnberg, Nanomaterialcharakterisierung (Streumethoden), Kristallographie und Strukturphysik, Staudtstraße 3, 91058 Erlangen, Germany.